Sensitivity analysis of a suspended CDPR to design parameters

Thibaut Paty, Nicolas Binaud, Stéphane Segonds

Sensitivity analysis of a suspended CDPR to design parameters

Thibaut PATY · Nicolas BINAUD · Stéphane SEGONDS

October 7, 2021

Abstract

1 Introduction

The Cable Driven Parallel Robots (CDPRs) are a particular type of parallel robots. It is a closed kinematic chains moved exclusively by cables [1]. They are promising systems due to their lightness, versatility and construction resistance [2]. They are composed by Moving-Platform (MP) attached with cables. These robots can be planar or spatial [3, 4] in function of the applications. Indeed, there are many types of applications, it is an already used system in stadium to film [5], this was the first commercial application of CDPRs. However, CDPRs are versatile systems. Many research works are seeking to adapt the CDPRs for different applications and environments. Many examples of use can be cited as the solar panel cleaning [6], the concret additive manufacturing of large parts [7], for the giant radio telescope [8] or also for haptic devices [9]. Suspended CDPRs are a system where the cables are exclusively coming from exclusively above the MP. The number of cables can be equal or less than the Degrees of freedom (Dof) in this case the CDPR is qualified of non-redundant [10]. In the case there are more cables than Dof it is named redundant [11]. For the suspended CDPRs, the gravity plays the role of a virtual cable which is always vertical. The study presented in this article focuses on the effect on CDPR error pose of the pulley architecture in relation to the mechanical parameters. Indeed, the MP pose error made when the mechanical parameter of the CDPR is neglected during the calculation of the unrolled cable. In the Paty's article [12] a novel pulley architecture has been introduced with a double revolute joint. The work presented in following publication analyzes the effect of the mechanical parameter on the CDPR equipped with two different pulleys and taking into account the cable sagging [13]. Indeed, the MP mass (m_{MP}), the cable linear mass (μ_0) and the Young's modulus (E) parameters have an impact on the CDPR control and moreover are subject to wide variation when using CDPR. The Young's modulus can be different during the use of the CDPR due to the aging, the hysteresis loop or its non-linearity [14]. Moreover, it is possible to differentiate the MP mass in two parts, the empty mass of the MP and the carried mass which can be vary during the CDPR use. In addition, for the same cable radius the linear mass of cable can be doubled depending on its construction.

The effects of these parameters, m_{MP}, μ_0, E and type of pulley joint, are analyzed on the global MP pose error through a Design Of Experiments (DOE) but also the evolution of the parameters effect as a function of the size of the CDPR. The objective is to determine if all factors are crucial during the CDPR design and if it is necessary to take all of them into account. The article is organized as follows: Section 2 introduces the models used, Section 3 presents the context of the study and finally Section 4 shows the results of the DOE and analyzes the effects evolution in relation to the size of the CDPR.

2 CDPR Modelling

2.1 Parametrization

The parametrization of the CDPR is essential. In this paper, two types of pulleys are studied and therefore

it is necessary to have one parametrization per pulley architecture. Therefore, at first, the parametrization of the single revolute joint pulley is presented then the double revolute joint pulley is set.

2.1.1 Single revolute joint pulley parametrization

Figure 1 presents the parametrization of the pulley designed with a single revolute joint. In this paper the CDPR equipped with this type of pulley is noted CDPR_{SR}.

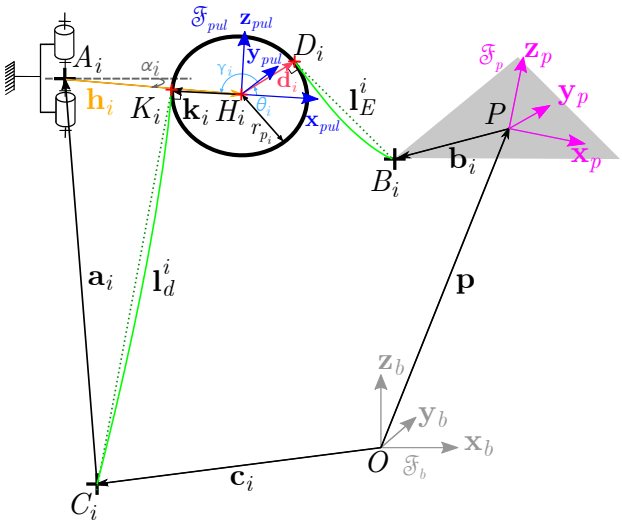

Figure 1: CDPR_{SR} parametrization with single revolute joint pulleys

The geometry of the pulley is described by a radius r_{p_i} and a lever arm of length h_i. This lever arm separates pulley centre H_i with the fixation point $A_i = [A_{i_x}\ A_{i_y}\ A_{i_z}]^T$ and it is described by the vector $\mathbf{h}_i$ (in orange in Fig. 1). The single revolute joint pulley can only turn according to $\mathbf{z}_b$, that gives him a Dof in the plan (A_i, $\mathbf{x}_b$, $\mathbf{y}_b$). To describe its orientation, α_i angle is defined. it is depending on the MP pose. The cable, plotted in green in Fig. 1, can be described in three parts, the dead length l_d^i between the winch represented by the C_i and the pulley entry point K_i, the cable wrapped around the pulley, and the useful cable lenght l_E^i between the pulley exit point D_i and the MP fixation point B_i. θ_i is the angle between $\mathbf{x}_{pul}$ and $\mathbf{d}_i$ where the vector $\mathbf{d}_i$ is the vector from H_i to D_i. In addition, γ_i is the angle between $\mathbf{d}_i$ and $\mathbf{k}_i$ which is the vector from H_i and K_i. The vector $\mathbf{p}$ describes the position of the MP centre into the base frame $\Im_b$ (in grey in Fig. 1). The MP has its own coordinate system described by the moving frame $\Im_p$ (in pink in Fig. 1). The pulley frame $\Im_{pul}$ (in blue in Fig. 1) is attached to the pulley. Note that b_i is expressed in $\Im_p$ and that k_i and d_i are expressed in $\Im_{pul}$.

2.1.2 Double revolute joint pulley parametrization

The general parametrization of the CDPR is the same as the one presented in the previous part. The difference is in the articulation of the pulley. Indeed, this pulley is composed with a double revolute joint. This articulation type allows two Dof in rotation, therefore its position must be described by two angles. The first angle is the same than the single revolute joint pulley, it is α_i describing its orientation around $\mathbf{z}_b$. The second angle is β_i, it allows to describe the pulley rotation between the plan (A_i, $\mathbf{x}_b$, $\mathbf{y}_b$) and $\mathbf{h}_i$ vector (see Fig. 2). In this paper the CDPR equipped with this type of pulley is noted CDPR_{DR}.

The parametrization of the different pulley architectures studied in this article has been described. The following section presents the strategy to compute the MP pose error made when the cable mass and elasticity are neglected.

2.2 Computed strategy of the MP pose error

Figure 3 presents the process used in the rest of the paper. This method is developed to analyze the error made when the cables mechanics are neglected for a MP pose. Firstly, it is necessary to determine the CDPR parameters and configuration. It is important to note that the MP is modelled like a mass point, defined by point P. This hypothesis means that the MP of the CDPR has only translation Dof and no rotation Dof. The next step is to calculate the total length of cable L_T^i necessary to reach the awaited

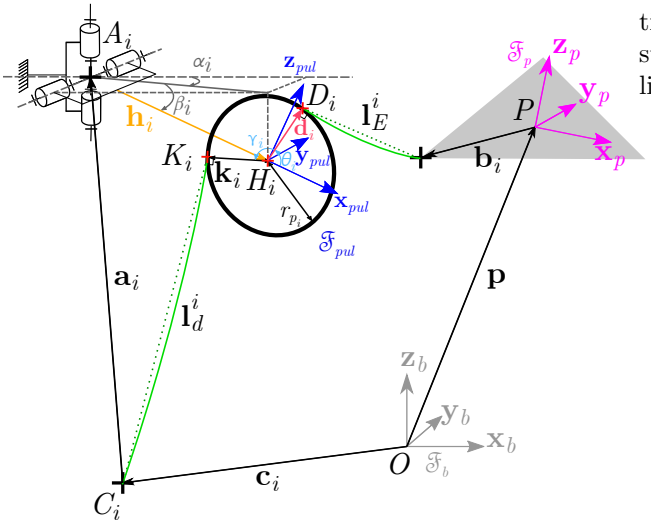

Figure 2: CDPR$_{DR}$ parametrization with double revolute joint pulleys

MP pose with the Extended Inverse Geometric Model (IGM$_E$) described in [12]. L_T^i is the addition of the useful length l_E^i, l_d^i and the winded cable on the pulley $\gamma_i r_{p_i}$. The set of L_T^i is noted $\mathbf{L}_T = [L_T^1, ..., L_T^i]^T$ where $i = 1, ..., m$. The IGM$_E$ does not take into account the elasticity and the mass of the cable and the MP mass. It is notified that two IGM$_E$ exist: one for the single revolute joint pulley and one for the double revolute joint. In this model the cable is considered as rigid segment. The values generated by IGM$_E$ are used to compute the Direct Catenary Model Extended (DCM$_E$) presented in section 2.4. The DCM$_E$ seeks the MP pose when the deployed cable is known and the cable mechanics is taken into account. In addition, the DCM$_E$ is solved numerically and it is why it is necessary to have a set of initial values determined in part by the IGM$_E$. However, it is also necessary to have a set of tension that it is not defined by IGM$_E$. To do this, a Tension Distribution Algorithm (TDA) is used in section 2.3 and generates an admissible set of tension $\mathbf{t}_{init}$. Once the initial values for the DCM$_E$ are determined, it is possible to calculate the vector position $\mathbf{p}_I$ for each architecture of pulley. $\mathbf{p}_I$ is the real MP pose when the cables lengths are affected by the mass and elasticity of cable and the mass of the MP. Using this strategy, the effect of the cable property can be highlighted.

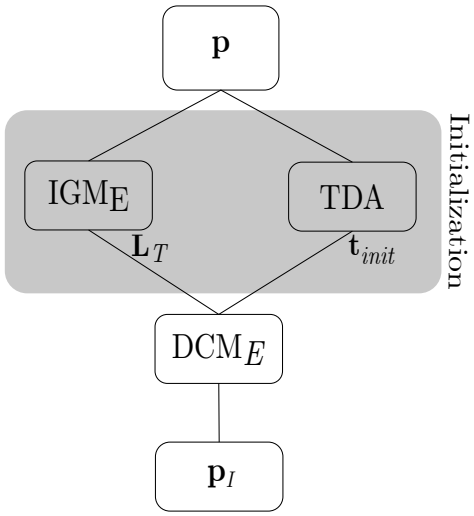

Figure 3: Diagram of the computed strategy

The calculation process is now presented, but it is necessary to express the different models and algorithms presented in this strategy. These methods are developed in the next parts. In first, the TDA is presented and after the DCM$_E$. It is noted that the IGM$_E$ is considered as presented in [12].

2.3 Tension Distribution Algorithm

To control a CDPR when it is redundant, a TDA is essential. Indeed, it is necessary to control the tensions in cables when there are more cables than Dof because there are several sets of tension that can be solutions. However, some solutions are not acceptable because they are negative tensions. Indeed, a cable can work exclusively in tension and cannot push the MP, this is why the tensions must be positive. There are many algorithms developed to manage the tensions [15, 16]. However, in this paper the TDA is used exclusively to determine the initial values of the optimization function to DCM$_E$, therefore is not necessary to have a complex algorithm. This is why

the TDA used in this article seeks to minimize the Euclidian norm of the tensions sum as in [17]. In addition, the tensions values are constrained with a lower boundary t_{min} and a superior boundary t_{max}. These boundaries allow to take into account the mechanical limits of the cable. Equation (1) shows the optimisation problem solving the TDA.

$$\begin{cases} \min \sqrt{\sum_{i=1}^{m} t_i^2} \\ t_i \geq t_{min} \\ t_i \leq t_{max} \end{cases} \tag{1}$$

Where t_i is the tension value in the cable i. This system of optimization is solved with an optimization function of Matlab named *fmincon*. To finalize the simulation strategy, the DCM$_E$ will now be explained.

2.4 Direct Catenary Model Extended

To model a cable of CDPR there are many models. Indeed, the cable can be modelled like:

1. a rigid body, its elasticity and mass are neglected [18];
2. a massless cable, it is represented as a segment and the Hook's law models its elongation [10];
3. a catenary, its elasticity and mass are considered, its sagging is modelled [19] ;

The present work seeks to know the effect of the cables Young's modulus, the mass of the MP and the linear mass of cable. To do so the catenary models are implemented using the Irvine's model [20] developed initially for the civil engineering field. This model has been adapted for the CDPRs. In this paper, two types of pulley architectures are investigated and it is therefore necessary to develop an equation system specific to each pulley. The system to calculate the DCM$_E$ in the case of the single revolute joint pulley is composed with $9m+3$ equations. Where m is the number of cables making the CDPR. In the case of the double revolute joint pulley, it is an equation system with $12m+3$ equations. Indeed, to compute the Irvine's model it is necessary to solve simultaneously, the tensions distribution, the static equilibrium of the CDPR and the constancy of the total length of cable deployed. It is the pulleys position equations that is the difference between the two systems. As for the TDA these systems are solved with the optimization function *fmincon* of Matlab.

2.4.1 DCM$_E$ with single revolute joint pulley

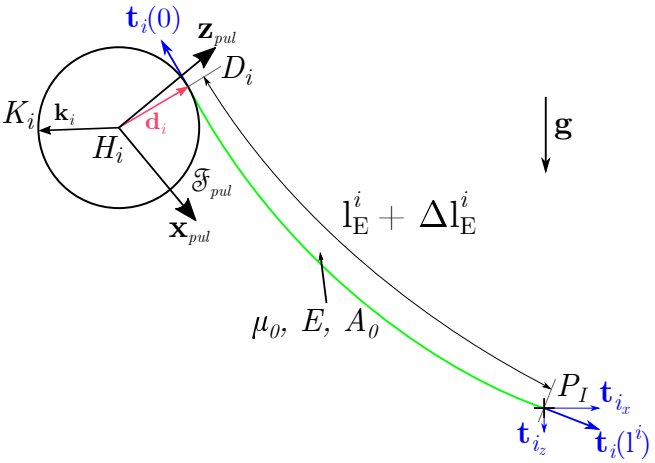

Figure 4: Diagram of sagging cable

In this part the system solving the DCM$_E$ for a CDPR$_{SR}$ is presented. The system can be decomposed into several groups of equations. First, the equations of Irvine's model [21] is developed. Young's modulus is considered like linear in the Irvine's model (see Fig. 4). Given that the dead length is taken into account, these equations are applied on two times, on the dead length l_d^i and on the useful length l_E^i. The equations that calculate the cable profile for useful length are:

$$\begin{cases} 0 = \frac{t_{i_x} l_E^i}{EA_0} + \frac{|t_{i_x}|}{\mu_0 g}[\sinh^{-1}(\frac{t_{i_z}}{t_{i_x}}) - \sinh^{-1}(\frac{t_{i_z} - \mu_0 g l_E^i}{t_{i_x}})] - x_{P_I} \\ 0 = \frac{t_{i_z} l_E^i}{EA_0} - \frac{l_E^{i2}\mu_0 g}{2EA_0} + \frac{1}{\mu_0 g}[\sqrt{t_{i_x}^2 + t_{i_z}^2} - \sqrt{t_{i_x}^2 + (t_{i_z} - \mu_0 g l_E^i)^2}] - \\ \qquad\qquad\qquad\qquad\qquad\qquad\qquad\qquad\qquad\qquad\qquad\qquad z_{P_I} \end{cases} \tag{2}$$

For the dead length the equations are:

$$\begin{cases} 0 = \frac{t_{di_x} l_d^i}{EA_0} + \frac{|t_{di_x}|}{\mu_0 g}[\sinh^{-1}(\frac{t_{di_z}}{t_{di_x}}) - \\ \qquad \sinh^{-1}(\frac{t_{di_z} - \mu_0 g l_d^i}{t_{di_x}})] - x_{K_i} \\ 0 = \frac{t_{di_z} l_d^i}{EA_0} - \frac{l_d^{i2}\mu_0 g}{2EA_0} + \frac{1}{\mu_0 g}[\sqrt{t_{di_x}^2 + t_{di_z}^2} - \\ \qquad \sqrt{t_{di_x}^2 + (t_{di_z} - \mu_0 g l_d^i)^2}] - z_{K_i} \end{cases} \tag{3}$$

Where t_{i_x}, t_{i_z} are the components of the vectors tension of useful cable $\mathbf{t}_i(l_E^i)$ and t_{di_x}, t_{di_z} the components for dead cable $\mathbf{t}_{di}(l_d^i)$. The models are expressed into the plan comprising the pulley and the cable, that is (H_i, $\mathbf{x}_{pul}$, $\mathbf{z}_{pul}$), it is why the vector position of the point P_I in $\Im_b$ is $\mathbf{p}_I = [x_{P_I}, 0, z_{P_I}]^T$ and the vector position of the point K_i in $\Im_{pul}$ is $\mathbf{k}_i = [x_{K_i}, 0, z_{K_i}]$. In addition, A_0, E and μ_0 are the mechanics parameters of the cable. A_0 is the section area of the cable, E is the Young's modulus and μ_0 is the linear mass. In these equations, the unknowns are: l_E^i, l_d^i, t_{i_x}, t_{i_z}, t_{di_x}, t_{di_z}, $\mathbf{p}_I$, $\mathbf{k}_i$. Newton's first law on the point P_I has to be verified to assure a static equilibrium of the cable tension (Eq. (4)).

$$\mathbf{0} = -\mathbf{W}_f \mathbf{t} + \mathbf{w}_{ext} \tag{4}$$

Where $\mathbf{w}_{ext}$ is the external wrench applied on the MP, $\mathbf{t}$ is the set of cables tensions as $\mathbf{t} = [\mathbf{t}_1, \ldots, \mathbf{t}_i]$ where $i = 1, \ldots, m$ and $\mathbf{W}_f$ is wrench matrix function of the MP pose.

Moreover, it is important to respect the constraint of tangency of cable to the entry and exit of the pulley. This is done by finding the perpendicularity between the cable vector and the pulley radius vector. Which means between the vector $\mathbf{d}_i$ and $\mathbf{l}_E^i$ for the useful part and between the vector $\mathbf{k}_i$ and $\mathbf{l}_d^i$ for the dead part. To do this, scalars products are implemented into the system Eq. (9) like in Eq. (5).

$$\begin{cases} 0 = \mathbf{d}_i . \mathbf{l}_E^i \\ 0 = \mathbf{k}_i . \mathbf{l}_d^i \end{cases} \tag{5}$$

As the objective of this models is to calculate the MP pose if the total length of cable is computed with an IGM$_E$. It is necessary to constraint the total length of cable remaining constant (Eq. (6)).

$$0 = l_d^i + l_E^i + \gamma r_p - L_T^i \tag{6}$$

To fit the static equilibrium of a cable it is necessary to have the same tension in the useful cable and the dead cable. In this article, the friction of the pulley is neglected. Indeed, it is considered that the pulley is equipped with ball bearing to reduce the friction. To do this, the Equation (7) is added to equalize the norm of tension between the pulley inlet (D_i) and the pulley outlet (K_i).

$$0 = \sqrt{t_{di_x}^2 + (t_{di_z} - \mu_0 g l_d^i)^2} - \sqrt{t_{i_x}^2 + (t_{i_z} - \mu_0 g l_E^i)^2} \tag{7}$$

Finally, it is necessary to determine the pulley pose with the α_i angle magnitude which is a function of the MP pose.

$$0 = tan^{-1} \frac{|A_{i_y} - z_P|}{|A_{i_x} - x_P|} - \alpha_i \tag{8}$$

Finally, the total equations to compute the DCME is detailed in system of equations (9).

$$
\begin{cases}
0 = \frac{t_{i_x} l_E^i}{EA_0} + \frac{|t_{i_x}|}{\mu_0 g}[\sinh^{-1}(\frac{t_{i_z}}{t_{i_x}}) - \\
\quad \sinh^{-1}(\frac{t_{i_z} - \mu_0 g l_E^i}{t_{i_x}})] - x_{P_I} \\
0 = \frac{t_{i_z} l_E^i}{EA_0} - \frac{l_E^{i2} \mu_0 g}{2EA_0} + \frac{1}{\mu_0 g}[\sqrt{t_{i_x}^2 + t_{i_z}^2} - \\
\qquad \sqrt{t_{i_x}^2 + (t_{i_z} - \mu_0 g l_E^i)^2}] - z_{P_I} \\
0 = \frac{t_{di_x} l_d^i}{EA_0} + \frac{|t_{di_x}|}{\mu_0 g}[\sinh^{-1}(\frac{t_{di_z}}{t_{di_x}}) - \\
\quad \sinh^{-1}(\frac{t_{di_z} - \mu_0 g l_d^i}{t_{di_x}})] - x_{K_i} \\
0 = \frac{t_{di_z} l_d^i}{EA_0} - \frac{l_d^{i2} \mu_0 g}{2EA_0} + \frac{1}{\mu_0 g}[\sqrt{t_{di_x}^2 + t_{di_z}^2} - \\
\qquad \sqrt{t_{di_x}^2 + (t_{di_z} - \mu_0 g l_d^i)^2}] - z_{K_i} \\
\mathbf{0} = -\mathbf{W}_f \mathbf{t} + \mathbf{w}_{ext} \\
0 = \mathbf{d}_i \cdot \mathbf{l}_E^i \\
0 = \mathbf{k}_i \cdot \mathbf{l}_d^i \\
0 = l_d^i + l_E^i + \gamma r_p - L_T^i \\
0 = \sqrt{t_{di_x}^2 + (t_{di_z} - \mu_0 g l_d^i)^2} - \sqrt{t_{i_x}^2 + (t_{i_z} - \mu_0 g l_E^i)^2} \\
0 = tan^{-1} \frac{|A_{i_y} - z_P|}{|A_{i_x} - x_P|} - \alpha_i
\end{cases}
\tag{9}
$$

2.4.2 DCM$_E$ with double revolute joint pulley

To compute the DCM$_E$ in the case of the double revolute joint pulley, it is necessary to complete the system of equations Eq. (9) to take into account the second joint. Like with the single revolute joint pulley, the friction is neglected, but also the mass of the pulley. Indeed, the tension of the cable is limited with a t_{min} which reduces the effect of the pulley mass [12]. Three equations per cables are added to compute the pulley pose. To do this, it is important to respect its static equilibrium. It is therefore necessary to find the position of the point M_i which is described by the position vector $\mathbf{m}_i = [x_{M_i}, 0, z_{M_i}]^T$. M_i is the intersection point of tensions vectors $\mathbf{t}_i(0)$ and $\mathbf{t}_i^d(l_d^i)$. Indeed, to respect the static equilibrium the vector $\mathbf{h}_i$ of the lever arm must pass by this point. To express the coordinate of M_i the parametric equation of the line $(D_i M_i)$ (Eq. (10)) and $(K_i M_i)$ (Eq. (11)) are used.

$$
\begin{cases}
x = x_{D_i} + t_{i_x} q_i \\
y = 0 \\
z = z_{D_i} + t_{i_z} q_i
\end{cases}
\tag{10}
$$

$$
\begin{cases}
x = x_{K_i} + t_{i_x}^d q_i' \\
y = 0 \\
z = z_{K_i} + t_{i_z}^d q_i'
\end{cases}
\tag{11}
$$

Where q_i and q_i' are the parameters of parametric equations. Therefore the equations added at the system Eq. (9) are the equations of Eq. (12).

$$
\begin{cases}
0 = h_i cos(\beta_i) + r_{p_i} cos(\theta_i^d - \beta_i) + t_{i_x}^d q_i' - x_{M_i} \\
0 = h_i sin(\beta_i) + r_{p_i} sin(\theta_i^d - \beta_i) + t_{i_z}^d q_i' - z_{M_i} \\
0 = tan^{-1} \frac{|z_{M_i}|}{|x_{K_i}|} - \beta_i
\end{cases}
\tag{12}
$$

In this section the DCM$_E$ has been presented for the two types of pulley articulation, the single and the double revolute joint. At the end of this process, many factors are known, including the pose P_I of the MP when the cables length was calculated with a model that does not take into account the sagging and the elasticity of cable.

2.5 MP pose error

To compare the influence of the parameters taken into account in the catenary models and not in the extended models it is necessary to use an index linking the both. This index is named $\|\delta \mathbf{p}\|$ it is the difference between the desired MP pose P and P_I the MP pose computed with DCM$_E$ (Eq. (13)).

$$
\|\delta \mathbf{p}\| = \|\mathbf{p}_I - \mathbf{p}\| \tag{13}
$$

This index, allows to observe the effects of the mechanics parameters of cable and MP on the

accuracy of the CDPR and translate the error made when these phenomena are neglected.

In this section, the parametrization of the CDPR, the DCM_E, the work process and the index of comparison $\|\delta\mathbf{p}\|$ are presented. Now, in the following section, the case study is presented and the effect of the Young's modulus, the MP mass, the cable linear mass and the type of pulley articulation is analyzed.

3 Study context

The methodology and models used in this paper being established, it is necessary to define a study case. This section set up the values used and the analyze field of this article. In first, the CDPR studied is described, then a method to determine the set of parameters defining the pulley is presented and finally the creation of a Common Regular Workspace (RW_C) is established. This methodology is presented for a CDPR of $15m$ square and $15m$ high noted CDPR_{15}, this method is used for different sizes of CDPR in final part of this paper.

3.1 Case study

In this paper, the studied CDPR is suspended with four cables [22]. The advantages of these architectures are that they free the ground and allow man/machine cohabitation. In addition, suspended architectures are more reconfigurable and more removable allowing the printing of building [23] or the personal rescue [24] to cite some applications. However, it is less resistant with respect to the effort oriented following $\mathbf{z}_b$ positive.

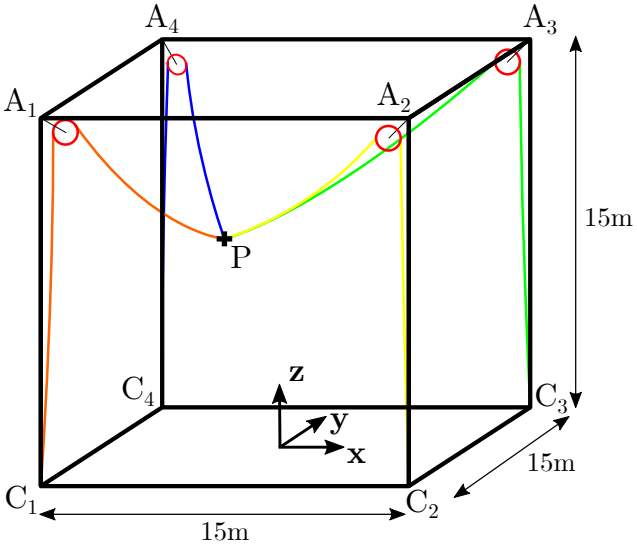

Figure 5: Schematization of the CDPR study with double revolute joint pulley

Figure 5 presents the studied CDPR. It is a CDPR with four cables, included in a cubic volume of side 15 meters. As presented in the section 2.1 the winch is modelled by C_i points localized at each corner of the CDPR. In this paper, these points are considered fixed and vertically aligned with A_i points. The MP is considered as a mass point and noted P. Given that the cables are modelled with a sagging model it is necessary to define its parameters. There are several values to be determined to have a realistic model. First, the cable radius r_c is established at $2mm$. In addition, a cable can be used within a given tension range between a t_{min} and t_{max}. Indeed, a cable is limited in maximal tension to remain in its elastic range. Moreover, if the tension is negative or too low the cable may unravel. These values are function of breaking load T_r with a value of $10.29kN$. In this study, the cables used are the Carl Stahl Technoscables Ref 1692. In these works, it is considered that cable tension is between 0.1% and 50% of maximum breaking load which means that $t_{min} = 10.29N$ and $t_{max} = 5145N$. Young's modulus, MP mass, linear mass and the type of pulley are studied but the other parameters are considered as constant. Firstly, the Young's modulus E of a cable is not constant be-

Lxlxh(m)	r_c(mm)	$\mu_0(kg.m^{-1})$	E(GPa)	m_{MP}(kg)
15x15x15	2	$[0.05; 0.1]$	$[67.2; 134.4]$	$[100; 200]$

Table 1: Parameters of the CDPR studied

cause a hysteresis phenomenon is present and moreover it can vary depending on whether the cable has been loaded or unloaded. These phenomena are difficult to model faithfully it is why they are studied using a DOE with a high value and low value in this paper. These limits are the lower and upper bound of the values that can be taken by E. Considering the experimental results presented in the Baklouti's article [14] and by extrapolating the values of E, an uncertainty of $70GP$ equally distributed around $102.2GPa$ is determined. This incertitude $\pm 35GPa$ allows to cover the whole range of variation of the elasticity. This gives as a low value $67.2GPa$ and for the high value $134.4GPa$. The high value is not exactly $102.2+35GPa$ because to improve the comparison, it was decided to use a high value as the double of the low one. In addition, this CDPR is in the idea dedicated to carrying variable loads. Indeed, generally a CDPR has a MP with an empty mass that is constant. However, the payload can be devoted to vary. Many uses generate a variability of payload such as personal assistance. In this use it is easy to imagine that the weight of a person is a highly variable value. The lower level is thus fixed at $100kg$ considered as the mass of the platform. The high level is set at $200kg$, considering the transport of people weighing up to $100kg$. Moreover, an important factor when a CDPR is designed is the choice of the cable type. Indeed, the manufacturing of cable implies a variation of linear mass for a same radius. In fact, there are several ways to strand a cable involving different linear masses. To observe the effect of the cable mass variation this value is integrated into the DOE. To choose the values of μ_0, the limits are fixed by comparing the different $2mm$ radius cables available from different manufacturers. Therefore, μ_0 is varying between $0.05kg.m^{-1}$ (for an cable with 6 strands of 7 wires in galvanized steel with textile core by LEVAC) and $0.1kg.m^{-1}$ (for a antigiratory cable with 19 strands of 7 wires galvanized steel with metallic core by J-Cardon & Fils). The individual strandings of the cables are shown in Fig. 6. In addition, the Tab. 1 resumes the CDPR studies in this article.

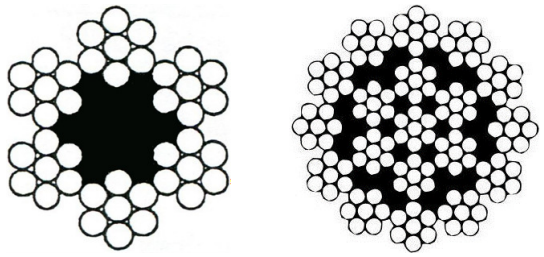

(a) Cable 6x7 in galvanized steel with textile core

(b) Antigiratory cable 19x7 in galvanized steel with metallic core

Figure 6: Stranding type of cables limiting μ_0

The parameters of the pulley are determined in the next part by a process to seek the best repeatability compared to E, m_{MP} and μ_0.

3.2 Optimal geometric pulley parameters

In this section it is sought the combination between r_p and h that improves the repeatability related to E, m_{MP} and μ_0. Indeed, r_p and h play an important role on the MP pose and on the effect of the E, m_{MP} and μ_0. In this section the mechanical parameters of the CDPR are fixed at the means values of their limits and only the geometric parameters describing the pulley are varing. The set of geometric parameters of r_p and h limiting the $\|\overline{\delta \mathbf{p}}\|$ is going to be searched for. This paper compares a model taking into account the pulley geometry with a model taking into account the

geometry pulley and also the sagging of cable. In this part, the $\|\overline{\delta \mathbf{p}}\|$ is calculated in the whole workspace for N different MP positions and the average pose error is determined, it is noted $\overline{\|\delta \mathbf{p}\|}$.

$$\overline{\|\delta \mathbf{p}\|} = \frac{1}{N} \sum_{i=1}^{N} \|\delta \mathbf{p}_i\| \tag{14}$$

To choose the r_p values it is necessary to respect the winding radius of cable. A ratio between r_p and r_c is evaluated and must be greater than 20 (Eq. (15)). All values of r_p tested respect this condition. In this study, the r_c is equal to $2mm$ it is implies that the minimum values of r_p is $40mm$. For the high level, it is considered that is the double of the lower level therefore $80mm$.

$$\frac{r_p}{r_c} \leq 20 \tag{15}$$

For the bound of h it is considered that h must respect the dimension constraint explained in Eq. (16). This constraint is used to ensure the proper functioning of the pulleys. Therefore, the values tested of r_p belong to the range $[40mm; 80mm]$ and the values of h are comprised into $[46mm; 86mm]$.

$$r_p + 3r_c \leq h \tag{16}$$

Figure 7 shows that the values of r_p and h generate the best results in terms of average of MP pose error. This value is noted $\overline{\|\delta \mathbf{p}\|}$ and defined as in Eq. (14). In this section the average of pose error is made on the total attainable workspace of each configuration CDPR. In the case of the CDPR$_{SR}$ (Fig. 7a) the minimum is spotted by a red circle. The best choice for r_p is $68.57mm$ and for h is $74.57mm$. Concerning the CDPR$_{DR}$ (Fig. 7b) the best result is located in the lower left part of the search set, and also spotted by a red circle. Therefore, the parameter set is r_p equal to $80mm$ and h equal to $86mm$. These values are sumarized in the Tab. 2.

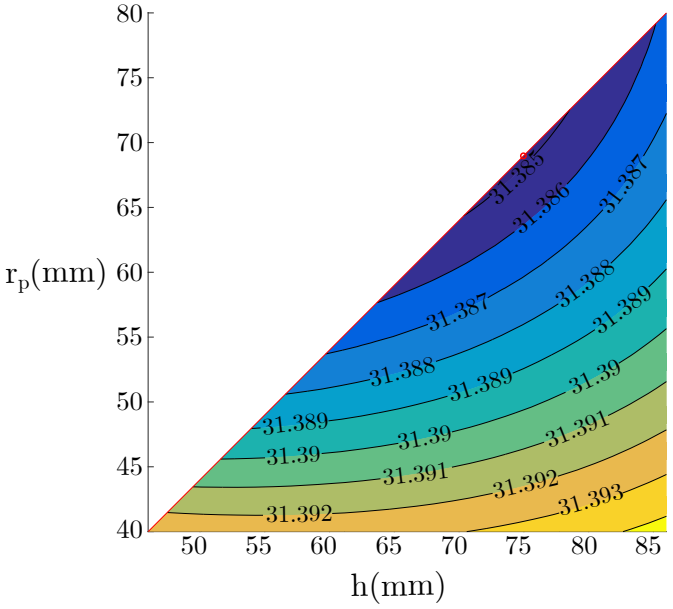

(a) CDPR$_{SR}$

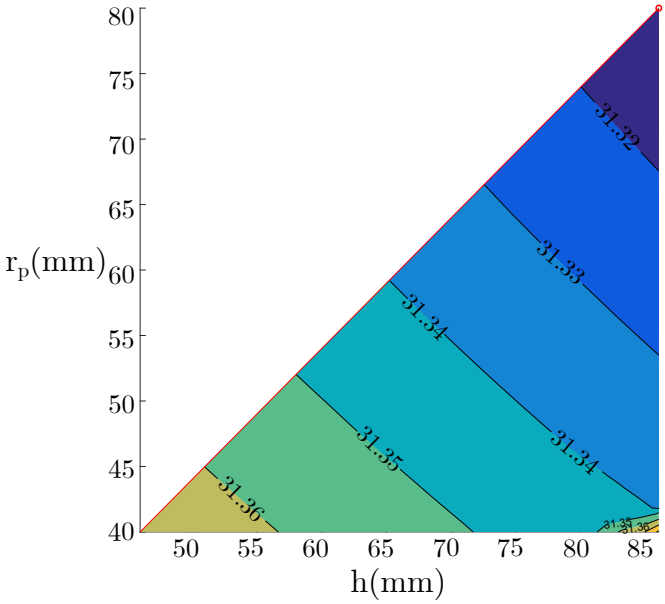

(b) CDPR$_{DR}$

Figure 7: Diagram of $\|\overline{\delta \mathbf{p}}\|$ (mm) in function of h and r_p

	CDPR_{SR}	CDPR_{DR}
r_p (mm)	68.6	80
h (mm)	74.6	86

Table 2: Values of the geometric pulley parameters

3.3 Common Regular workspace

The geometric values of the CDPR are fixed, now it is necessary to determine a space where it is possible to compare on the same number of points the different tests. This space is named Common Regular Workspace (RW_C) [25]. It allows to describe a volume where the CDPR can work easily and continuously. It is a geometric shape included in whole workspaces of the all test of the DOE. In this paper, the shape of RW_C is a cuboid. The RW_C shape is selected in function of the CDPR shape. To determine is dimensions it is necessary to compute many tests, presented into the next section. For each, the own regular workspace (RW^j, $j = 1 \ldots 16$) is calculated, looking for the largest possible cuboid. To find the RW^j, it seeks the rectangle maximizing its aera for each height of the CDPR workspace and the smallest is chosen. As noted in the reminder of the paper, the study will focus only on a quarter of the CDPR because of the existing symmetries. This operation is carried out on all the different configurations on and the intersection of all RW^j is considered as RW_C. Figure 8 shows the RW_C into the own workspace of test 2 because it is the test that minimize the RW_C. The rectangles limiting the workspace are squares and are generated by tests 2 and 5. The dimension of the square is $6.74m$ of length. It is possible to observe that the bottom in Fig. 8 of their workspace is greatly reduced by the presence of tension lower than t_{min} in the opposite cable. Moreover, the first observation is that when the m_{MP} is low the RW are reduced, impacting the dimensions of the RW_C. In addition, the largest base square is generated by the CDPR equipped with a double revolute joint and a m_{MP} with a high value (tests 11, 12, 14 and 15). Concerning the vertical limit, it is defined by many tests (tests 1, 2, 3, 4, 6, 7, 11, 12, 14 and 15), the value is $12m$.

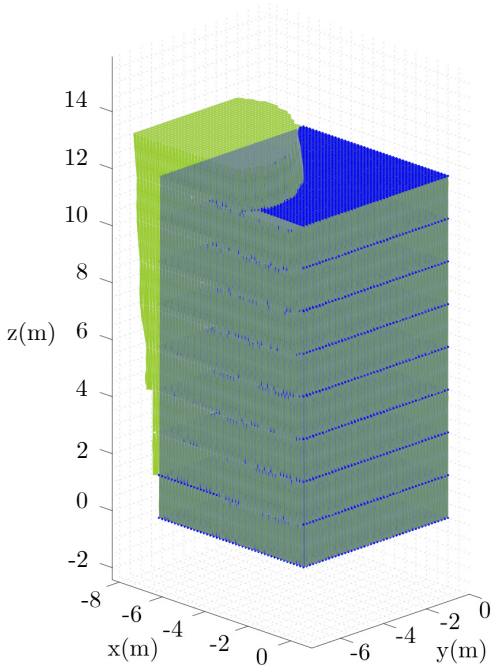

Figure 8: The RW_C include in the quart own workspace of tests 2

In this section the context of the study has been presented and the factor m_{MP} plays an important role on the workspace. The articulation type seems to plays also a role on the attainable workspace. Moreover, the geometric parameters must be chosen to reduce the effect of the E and m_{MP}. CDPR parameters and analyzes tools are now established. The next section analyses the MP pose error with a DOE and the workspace for different pulley architectures.

4 Effect of variability of payload and sagging of the cable

The study seeks to determine the effects of E, m_{MP}, μ_0 and joint type on the MP pose error. In following section 2.5 the models and the computing strategies are established. In section 3.3 the CDPR study is defined and the RW_C is delineated. In this part, it seeks

with a DOE the effects of E, m_{MP}, μ_0 and joint type are analyzed. Finally, the evolution of these effects is analyzed in function of the CDPR dimension.

4.1 Design of experiment

Firstly, the experiment planning is presented. The DOE is a way to analyze the effect and interaction between several parameters. In the case of this study, the parameters are E the Young's modulus of cable, m_{MP} the MP mass, the linear mass of cable μ_0 and the type of pulley articulation. The values defining the boundaries of the DOE are the same as those defined in the section 3.1 and are reminded in Tab. 3. In order to extract all effects and interactions of the four studied parameters, the complete 16-tests DOE is performed. Table. 3 summarizes the DOE and defines the different tests carried out to evaluate the effects and interactions of the studied parameters.

As in the previous section the study is led on the quarter of the CDPR. To compare and compute the effects and interactions it is necessary to determine a value as response of the DOE. The average of the MP pose error on the RW_C $\overline{\|\delta\mathbf{p}\|}$ is used as a response. It is determined as in section 2 by the Eq. (14) with the only exception that N is fixed whatever the tests. Indeed, in this paper it is sought to compare and quantify the effect of the parameters on the MP pose error and not on the attainable workspace. It is why, this DOE is not applied on the total volume of CDPR but only on the RW_C defined in section 3.3. Indeed, to allow to compare each test between them, it is necessary to observe on the same number of point N. To do this the RW_C defined previously is discretised in ten heights and each height is composed of 2601 points thus N is equal to 26010.

The DOE is now defined and the tests are established. In the next part, the effect and interactions are presented and analyzed.

4.2 Results of design of experiment

As previously presented the studied response of the DOE is $\overline{\|\delta\mathbf{p}\|}$. Using these results the effects and interactions can be determined.

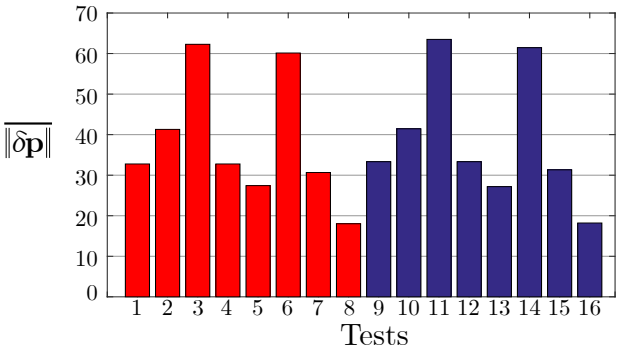

Figure 9: The values $\overline{\|\delta\mathbf{p}\|}$ for each test of the DOE

Figure 9 shows the $\overline{\|\delta\mathbf{p}\|}$ of each test. The eight first test are CDPR_{SR}s (in red in Fig. 9) and the eight last are CDPR_{DR}s (in blue in Fig. 9). The first observation is that the values are generally the same in the case of CDPR_{SR} that CDPR_{DR}. Indeed, the means of the $\overline{\|\delta\mathbf{p}\|}$ CDPR_{SR} is equal to $38.3mm$ and $38.5mm$ for the CDPR_{DR}. Thus, the type of joint seams to play a neglected effect when the cable lengths are computed with a IGM_E. This can be explained by having selected the optimal geometric dimension of the pulley in section 2. It is clear that the different factors have the same effect on the two types of pulley joint. Therefore, the configurations that generates the best results are 8 and 16. Indeed, this corresponds to a cable with a high E and a low m_{MP} and μ_0 with low mass. Similarly, the two tests where $\overline{\|\delta\mathbf{p}\|}$ is the highest are the tests 3 and 11. These tests are equivalent to the inverse of the best configuration, that is to say to a cable with a low E and a high m_{MP} and μ_0 with high mass. These observations are trivial, in fact when the cables are rigid with low masses, it is better than very elastic cables with high masses. Therefore, it is interesting to analyze the effect and interaction in more details. In Fig. 10, it is shown the effect of each factor. The observation is that the evolution of E leads to a decrease of $\overline{\|\delta\mathbf{p}\|}$ and inversely for m_{MP} and μ_0 when these values increase they have a negative impact $\overline{\|\delta\mathbf{p}\|}$. The effect of E is more important than m_{MP} and μ_0. However, the absolute effect of E ($11.1mm$) is equivalent to the sum of the effects of m_{MP} and μ_0 ($11.2mm$). So, if and only if E is high,

N^o	Joint	E	m_{MP}	μ_0
1	-1	-1	-1	-1
2	-1	-1	-1	+1
3	-1	-1	+1	+1
4	-1	+1	+1	+1
5	-1	+1	-1	+1
6	-1	-1	+1	-1
7	-1	+1	+1	-1
8	-1	+1	-1	-1
9	+1	-1	-1	-1
10	+1	-1	-1	+1
11	+1	-1	+1	+1
12	+1	+1	+1	+1
13	+1	+1	-1	+1
14	+1	-1	+1	-1
15	+1	+1	+1	-1
16	+1	+1	-1	-1
Field of study				
Level -1	1 joint	$67.2GPa$	$100kg$	$0.05kg.m^{-1}$
Level +1	2 joints	$134.4GPa$	$200kg$	$0.1kg.m^{-1}$

Table 3: Full factorial DOE with four factors

it can compensate the influence of the masses. In addition, the effect of the type of joint plays a neglected role on $\overline{\|\delta\mathbf{p}\|}$ against to E, m_{MP} and μ_0.

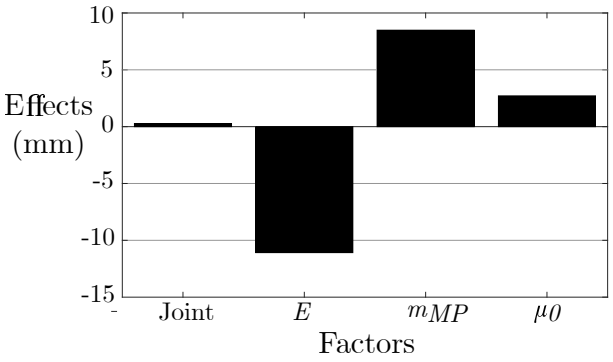

Figure 10: Effects of the factors

Figure 11 shows the interactions between pairs of factors communally named the first order interaction.

The interactions between the joint type and E, the joint type and m_{MP} and the joint type and μ_0 are also negligible in comparison to the interaction between E and m_{MP} and between m_{MP} and μ_0. Indeed, the interaction between E and m_{MP} is the greater interaction ($3.82mm$). Moreover, this interaction is greater than the only effect of μ_0 ($2.7mm$). The second important interaction is the one between m_{MP} and μ_0 indicating a link between the masses. This implies that the linear mass of the cable is not negligible contrary to what could be wrongly stated looking only at in Figure 10.

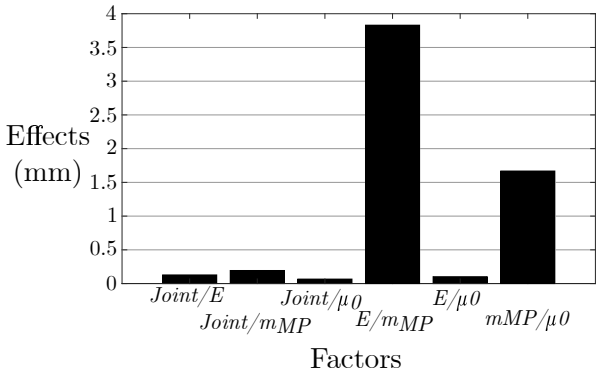

Figure 11: First order interactions of the factors

Figure 12 shows the interactions three by three of the factors and the interaction between all parameters. By analysing the values these interactions can be neglected compared to the effects or the second order interactions.

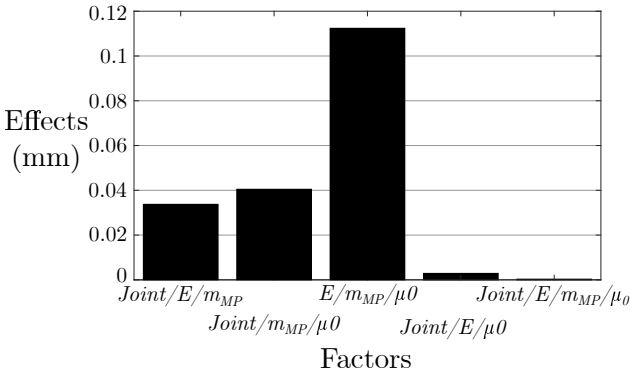

Figure 12: Second and third order interactions of the factors

Therefore, the mechanical parameters of the CDPR play a role more important than the geometric ones and it is the parameters that are the most subject to the variation during the use of the CDPR. For a CDPR_{15} it is necessary to consider the elasticity of the cable and the MP mass to have a reasonable accuracy of the MP. However, the μ_0 is also an important factor on the MP pose error. It is why it is important to consider this variation and the range of use of the CDPR during the design of CDPR. Until now it is a CDPR_{15} that has been studied in the next part, the evolution of each effect of the factors with respect to the CDPR dimension is studied.

4.3 Evolution of the parameters effects in function of CDPR dimension

It is observed that the effects of E, m_{MP} and μ_0 are not neglected for a CDPR_{15} when cables lengths are computed with an IGM_E. Now, it is studied the influence of the CDPR dimensions. The processes presented in section 2 and 3.3 are applied on different CDPR dimensions. The dimension of CDPR studied are presented in Tab. 4 showing geometric pulleys dimensions defined as in section 2. A RW_C for each CDPR dimensions is defined and the DOE described in Tab. 3 is applied. This series of computation allows to compile the effects for the different factors and plot them (Fig. 13). This representation allows to observe the evolution of the effects and conclude on the necessity to take or not a factor in the CDPR model. To make easier the comparison the absolute values of the effect of E are represented.

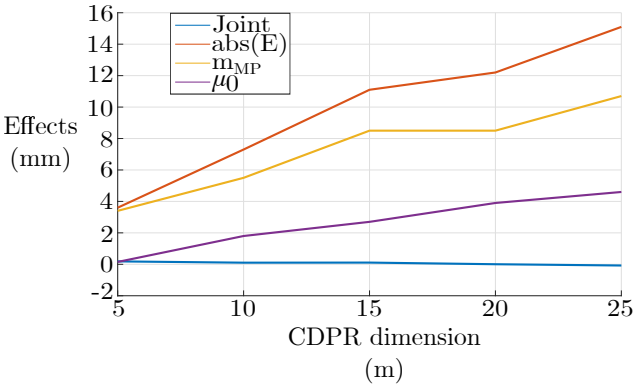

Figure 13: Evolution of the effects of each factors in function of CDPR dimensions.

The first observation on Fig. 13 it that the absolute values of Young's modulus E is always the factor with the highest effect. In addition, the effect of absolute values of E is almost the same that for m_{MP} for a CDPR_5. Thereafter, the evolution of E

CDPR notation		$CDPR_5$	$CDPR_{10}$	$CDPR_{15}$	$CDPR_{20}$	$CDPR_{25}$
lxLxH (m)		5x5x5	10x10x10	15x15x15	20x20x20	25x25x25
$r_p(mm)$	Single	80	80	68.57	40	40
	Double	80	80	80	42.86	42.86
$h(mm)$	Single	86	86	74.57	46	46
	Double	86	86	86	86	86

Table 4: Values of the CDPR dimensions and the optimal geometric values describing the pulleys of the CDPRs studied

is greater than m_{MP} which means E is more influential on the average of MP pose error for the other CDPR dimensions. Moreover, the effect of μ_0 takes more and more importance when the CDPR grows. Indeed, for a little CDPR the linear masses of cable are less influence because the cable length deployed is too short. However, from $CDPR_{10}$ it is necessary to take into account the linear mass μ_0. Indeed, for a $CDPR_5$ this factor is less influential than the articulation, that means for a $CDPR_5$ it useful to modelling the pulley articulation and not necessarily the cable mass linear. This observation can be explained by the important effect of μ_0 in sagging phenomena of cable, thus for the $CDPR_5$ this phenomenon is reduced by the short dimension of cable but cannot be overlooked for larger CDPRs. However, the effect of articulation is negligible for the other CDPR dimensions. These observations allow to determine easily the necessity to take or not into account a factor during the CDPR preliminary design and knower easily the effect of each mechanical factor for a CDPR cubic dimension.

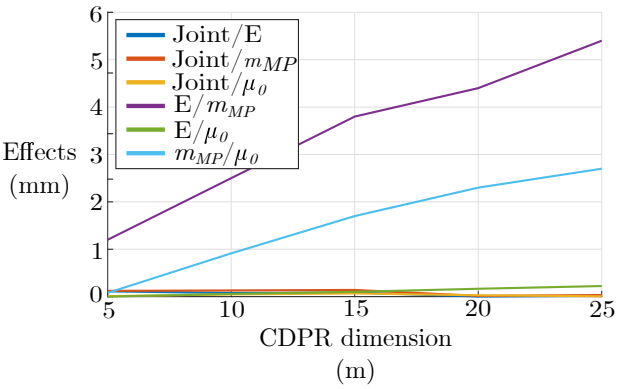

Figure 14: Evolution of the first order interaction between factors in function of CDPR dimensions.

Figure 14 presents the interactions between two factors in function of the CDPR dimensions. Two interactions are important: the interaction between E and m_{MP} and between m_{MP} and μ_0 stand out from the others. The other interactions are negligleable on all CDPR dimensions. More specifically, the interaction between m_{MP} and μ_0 is minor for a $CDPR_5$. However, for the other dimensions it becomes relatively important and this is even more true for the interaction between E and m_{MP}. Indeed, when Fig. 14 is compared with Fig. 13 it appears that this values is always higher than the effect of μ_0. This because the elongation of cable is principally imposed by the E and the mass. This mass is composed by the m_{MP} and μ_0, in these two mass the m_{MP} is always much higher than μ_0. It is why the interaction between E and m_{MP} is greater than the interaction E and μ_0 (in green on Fig. 14). The interaction between m_{MP} and μ_0 can be explained by the sagging effect of cable. Indeed, an evolution of μ_0 and m_{MP} plays a role on sagging but also on elongation of cable thus an evolution of the two factors have a conjugated effect on $\overline{\|\delta\mathbf{p}\|}$. Figure 14 represents the importance of the interaction between factors and shows that some of them cannot be neglected.

5 Conclusion

This paper deals with the modelling of cable-driven parallel robots (CDPRs) while considering pulley kinematics and the sagging of cables. The extended catenary models are used to analyze the MP pose error in regards to the extended geometric static models. A process of selection of the set of pulley parameters allowing to minimize the average MP pose error and the seek RW_C allowing the application of design of experiment and the results comparison is developed. The influence on the MP pose error of the pulley articulation, of E, of m_{MP} and μ_0 are studied with this design of experiment. Afterwards, these effects are analyzed in function of the CDPR dimensions. Firstly, results show that when the pulley dimension are selected the effect of the type of pulley articulation are negligible, except for the case of a little CDPR. In addition, the linear mass of cable plays a negligible effect for a small CDPR then its effect becomes more and more important according to the CDPR dimensions. The mass of the MP has an important effect for all CDPR dimensions and its evolution is less significant than for E. Indeed, E have the strongest effect on $\overline{\|\delta\mathbf{p}\|}$, the evolution of E allows a decrease of the MP pose error.

To conclude, this paper has highlighted the necessity to take into account many factors during the CDPR design. Indeed, for all dimensions of CDPR the Young's modulus of cable and the MP mass are crucial in the modelling. In addition, the linear mass of cable is a factor that needs to be taken into account for robots with large dimensions. However, the articulation type is relatively negligible when the cables lengths are computed with an extended model. In addition, first order interaction between the important factors must be taken into account.

Future work will focus on the modelling of the nonlinearity of E and its variation in each cable. The position of the A_i points must be optimized to minimize the $\overline{\|\delta\mathbf{p}\|}$ in a chosen RW_C.

References

1. Carpio MA, Placencia JC, Aller JM, Saltarén RJ, Rodríguez A, Portilla GA, and Cely JS. Modeling and Oscillations Control of a Planar Parallel Robot Subsystem Activated by Cable. *2019 IEEE 4th Colombian Conference on Automatic Control (CCAC).* 2019 :1–5. DOI: 10.1109/CCAC.2019.8920840
2. Merlet JP. Parallel robots second edition. Springer-Verlag New York Inc., 2006
3. Rasheed T, Long P, Marquez-Gamez D, and Caro S. Available Wrench Set for Planar Mobile Cable-Driven Parallel Robots. *2018 IEEE International Conference on Robotics and Automation (ICRA).* 2018 :962–7. DOI: 10.1109/ICRA.2018.8461199
4. Gagliardini L, Caro S, Gouttefarde M, and Girin A. A reconfiguration strategy for reconfigurable cable-driven parallel robots. *2015 IEEE International Conference on Robotics and Automation (ICRA).* 2015 :1613–20. DOI: 10.1109/ICRA.2015.7139404
5. Passarini C, Zanotto D, and Boschetti G. Dynamic Trajectory Planning for Failure Recovery in Cable-Suspended Camera Systems. en. Journal of Mechanisms and Robotics 2019 Apr; 11:021001. DOI: 10.1115/1.4041942. Available from: https://asmedigitalcollection.asme.org/mechanismsrobotics/article/doi/10.1115/1.4041942/472346/Dynamic-Trajectory-Planning-for-Failure-Recovery [Accessed on: 2021 Jan 29]
6. S.Seriani, Gallina P, and Wedler A. A modular cable robot for inspection and light manipulation on celestial bodies. Acta Astronautica 2016; 123:145–53. DOI: 10.1016/j.actaastro.2016.03.020
7. Izard JB, Dubor A, Herve PE, Cabay E, Culla D, Rodriguez M, and Barrado M. On the improvements of a cable-driven parallel robot for achieving additive manufacturing for construction. *Cable-Driven Parallel Robots. Mechanisms*

and Machine Science. Vol. 53. 2018. DOI: 10.1007/978-3-319-61431-1_30

8. Duan B. A new design project of the line feed structure for large spherical radio telescope and its nonlinear dynamic analysis. Mechatronics 1999; 9:53–64. DOI: 10.1016/S0957-4158(98)00028-2
9. Perreault S and Gosselin C. Cable-driven parallel mechanisms: application to a locomotion interface. Journal of Mechanical Design 2008; 130:102301. DOI: 10.1109/ICRA.2015.7139404
10. Baklouti S, Caro S, and Courteille E. Elasto-dynamic Model-Based Control of Non-redundant Cable-Driven Parallel Robots. *Dynamics and Control. CISM International Centre for Mechanical Sciences, Springer*. Vol. 584. 6. 2019 :238–46. DOI: http://link.springer.com/10.1007/978-3-319-78963-7_31
11. Mikelsons L, Bruckmann T, Hiller M, and Schramm D. A real-time capable force calculation algorithm for redundant tendon-based parallel manipulators. *2008 International Conference on Robotics and Automation*. 2008 :3869–74. DOI: 10.1109/ROBOT.2008.4543805
12. Paty T, Binaud N, Caro S, and Segonds S. Cable-driven parallel robot modelling considering pulley kinematics and cable elasticity. Mechanism and Machine Theory 2021; 159. DOI: 10.1016/j.mechmachtheory.2021.104263
13. Merlet J. Singularity of Cable-Driven Parallel Robot With Sagging Cables: Preliminary Investigation. *2019 International Conference on Robotics and Automation (ICRA)*. 2019 :504–9. DOI: 10.1109/ICRA.2019.8794218
14. Baklouti S, Caro S, and Courteille E. Sensitivity analysis of the elasto-geometrical model of cable-driven parallel robots. *Cable-Driven Parallel Robots*. Springer International Publishing, 2018 :37–49. DOI: 10.1007/978-3-319-61431-1_4
15. Gouttefarde M, Lamaury J, Reichert C, and Bruckmann T. A Versatile Tension Distribution Algorithm for n-DOF Parallel Robots Driven by n + 2 Cables. *IEEE Transactions on Robotics, IEEE*. Vol. 31. 6. 2015 :1444–57. DOI: 10.1109/TRO.2015.2495005
16. Cote AF, Cardou P, and Gosselin C. A tension distribution algorithm for cable-driven parallel robots operating beyond their wrench-feasible workspace. *2016 16th International Conference on Control, Automation and Systems (ICCAS)*. 2016 :68–73. DOI: 10.1109/ICCAS.2016.7832301
17. Bruckmann T, Pott A, Franitza D, and Hiller M. A Modular Controller for Redundantly Actuated Tendon-Based Stewart Platforms. *EuCoMes, The First Conference on Mechanism Science*. 2006 :1–12
18. Picard E, Caro S, Pleastan F, and Claveau F. Control Solution for a Cable Driven Parallel Robot with Highly Variable Payload. *ASME 2018 International Design Engineering Technical Conferences and Computers and Information in Engineering Conference*. 2018 :1429–36. DOI: 10.1115/DETC2018-85304
19. Merlet J. Computing cross-sections of the workspace of cable-driven parallel robots with six sagging cables. *CK 2017 - Computational Kinematics*. 2017 :182–9. DOI: 10.1007/978-3-319-60867-9_21
20. Irvine HM. Cable Structures. The MIT Press Series in Structural Mechanics, 1981
21. Riehl N, Gouttefarde M, Kurt S, Baradat C, and Pierrot F. Effects of non-negligible cable mass on the static behavior of large workspace cable-driven parallel mechanisms. *2009 IEEE International Conference on Robotics and Automation*. 2009 :2193–8. DOI: 10.1109/ROBOT.2009.5152576
22. Hanafie J, Nurahmi L, Caro S, and Pramujati B. Design optimization of spatial four cables suspended cable driven parallel robot for rapide life-scan. *AIP Conference Proceedings*. Vol. 1983. 1. 2018. DOI: 10.1063/1.5046299

23. Phuoc TT and Truong TN. Using a Cable-Driven Parallel Robot with Applications in 3D Concrete Printing. Applied Sciences 2021; 11. DOI: 10.3390/app110205638

24. Merlet J. Checking the cable configuration of cable-driven parallel robots on a trajectory. *2014 IEEE International Conference on Robotics and Automation (ICRA)*. 2014 :1586–91. DOI: 10.1109/ICRA.2014.6907063

25. Binaud N, Caro S, and Wenger P. Sensitivity comparison of planar parallel manipulators. Mechanism and Machine Theory 2010; 45:1477–90. DOI: 10.1016/j.mechmachtheory.2010.07.004